Corrosion Science 187 (2021) 109514

Contents lists available at ScienceDirect

Corrosion Science

journal homepage: www.elsevier.com/locate/corsci

Study of cathodic reactions in defects of thermal spray aluminium coatings on steel in artificial seawater

R. Grinon-Echaniz [a,b], P. Refait [c], M. Jeannin [c], R. Sabot [c], S. Paul [a,d,*], R. Thornton [a]

[a] School of Engineering, University of Leicester, University Road, Leicester, LE1 7RH, United Kingdom
[b] NSIRC, Granta Park, Cambridge, CB21 6AL, United Kingdom
[c] LaSIE Laboratory, UMR 7356 CNRS - La Rochelle University, Bât. Marie Curie, Avenue Michel Crépeau, 17000 La Rochelle, France
[d] TWI, Granta Park, Cambridge, CB21 6AL, United Kingdom

ARTICLE INFO

Keywords:
A – Aluminium
A – Carbon steel
A – Metal coatings
B – EIS
B – Electrochemical calculation
C – Cathodic protection

ABSTRACT

Electrochemical and surface characterization techniques were used to study the corrosion protection provided by Thermal Spray Aluminium (TSA) coatings on carbon steel substrates with and without defects in artificial seawater. Results showed that the presence of defects accelerates the formation of a protective corrosion product layer on the TSA coating. Voltammetry and Electrochemical Impedance Spectroscopy (EIS) revealed that both calcareous deposits and aluminium corrosion products hindered diffusion of dissolved O_2. Analysis of corrosion products by SEM-EDX, μ-Raman spectroscopy and XRD revealed Al oxides/hydroxides and hydrotalcite on top of TSA coating and a bilayer of calcareous deposits on the defect area.

1. Introduction

Corrosion of carbon steel is a serious problem for the offshore industry. The high yield strength and low cost of this material makes it desirable to build oil and gas platforms, ships, wind turbine monopiles, pipelines or bridges. However, its resistance to corrosion is limited, resulting in severe degradation in marine environments. High chloride levels, dissolved oxygen, fluctuating temperatures, sun's UV light and microbial species are some of the factors leading to high corrosion rates in marine environments. Material degradation under these conditions results in high costs of maintenance and repair of damaged areas, as well as high risks of premature catastrophic failures. Therefore, in order to reduce costs and provide safer structures, mitigation of corrosion is often achieved by sacrificial anodes, impressed current and/or coatings [1–3].

Thermal spray coatings (mainly Al and Zn alloys) have been successfully applied for decades to minimize corrosion losses in marine environments [4–6]. Arc spray and flame spray methods are the most common ones to produce thermal spray coatings for marine applications. In addition to a physical barrier, due to their less noble potential, they are able to provide cathodic polarization to the underlying steel. One of the earliest examples of thermal spray aluminium (TSA) in service was in 1984 in the North Sea. TSA was applied on the Hutton Tension Leg Platform, and inspection after 8 years of service showed the coating was in excellent conditions with no evidence of corrosion or damage to the substrate. Since then, international standards have been created for the application of thermal spray coatings for the corrosion protection of steel [7].

Existing studies have indicated that TSA coatings are able to provide cathodic protection of steel substrates under immersed conditions in marine environments for 20–30 years [5,8–10]. TSA acts as an anode and is consumed in order to protect steel (Eq. 1), whereas Eq.s 2 (oxygen reduction) and 3 (hydrogen evolution) take place on cathodic sites. However, as we can see from the standard potential values (E^o), Eq. 2 is the predominant cathodic reaction as Eq. 3 is less thermodynamically favourable.

$$Al^{3+}(aq) + 3e^- \rightarrow Al(s);\ E^o = -1.66\ V\ SHE \quad (1)$$

$$O_2(g) + 2H_2O(l) + 4e^- \rightarrow 4OH^-(aq);\ E^o = +0.40\ V\ SHE \quad (2)$$

$$2H_2O(l) + 2e^- \rightarrow H_2(g) + 2OH^-(aq);\ E^o = -0.83\ V\ SHE \quad (3)$$

Over time, the formation of Al oxides/hydroxides on the TSA surface reduces its self-corrosion [11,12]. In addition, in defect areas where the steel substrate is exposed, the release of OH^- (Eq.s 2 and 3) on the

* Corresponding author at: School of Engineering, University of Leicester, University Road, Leicester, LE1 7RH, United Kingdom; TWI, Granta Park, Cambridge, CB21 6AL, United Kingdom.
E-mail addresses: rge4@le.ac.uk (R. Grinon-Echaniz), prefait@univ-lr.fr (P. Refait), marc.jeannin@univ-lr.fr (M. Jeannin), rene.sabot@univ-lr.fr (R. Sabot), shiladitya.paul@twi.co.uk (S. Paul), rob.thornton@le.ac.uk (R. Thornton).

https://doi.org/10.1016/j.corsci.2021.109514
Received 2 November 2020; Received in revised form 16 April 2021; Accepted 27 April 2021
Available online 29 April 2021

Table 1
Thermal spray process parameters.

Wire diameter [mm]	Wire Feed Rate [m min^{-1}]	Spray Distance [mm]	Increment Step [mm]	Traverse speed [m s^{-1}]	Voltage [V]	Nominal Thickness [μm]
2.3	5.0	95.0	10.0	0.45	33.0	200−300

Table 2
Nominal composition of carbon steel (S355 N, EN 10,025-3:2004) substrates.

Elements	C	Mn	Si	P	S	Cr	Ni	Cu	Al	Mo
Wt. %	0.150	1.350	0.030	0.016	0.005	0.080	0.060	0.170	0.035	0.014

cathodic steel surface modifies the local pH and promotes the formation of calcareous deposits [13–15]. Therefore, in order to evaluate the performance of these coatings in the laboratory, it is important to perform tests in artificial (or real) seawater containing ions such as Ca^{2+}, Mg^{2+} and SO_4^{2-}, which are crucial for the formation of corrosion deposits [10,15–17].

Although TSA coatings are frequently used to protect offshore steel structures, the corrosion protection mechanism is not fully understood. In the literature, different methods have been reported to evaluate corrosion performance of thermal spray coatings by means of corrosion rates [6,9]. However, an in depth electrochemical study of the corrosion mechanism of TSA samples with defects comparing several techniques is lacking. Existing literature also lacks an in-depth examination of the effects associated with the presence of defects on the TSA coatings. Previous studies show either artificial defects machined on thermally sprayed coatings or two separate plates recreating the coating and the substrate [10,18–20]. Under these approaches, either the anodic and cathodic processes cannot be differentiated or the geometry of the samples has been altered. In order to be able to evaluate the performance of damaged TSA coatings in marine environment, it is necessary to separate the anodic and cathodic processes while keeping the geometry of real service exposure. For this purpose, we introduce a new methodology to prepare TSA samples with defects. We designed a bi-electrode where TSA coating and steel substrate are not in physical contact but keep the same geometry as TSA with defects that are caused by erosion, microbial influence or mechanical damage in service. The two parts of the bi-electrode (TSA coated part and bare steel part) can then be studied separately, i.e. electrochemical measurements such as EIS can be performed on each part independently.

In the present study, a combination of electrochemical techniques (OCP measurements, EIS and voltammetry), a new methodology to prepare TSA samples with defects and surface analysis techniques (SEM/EDX, XRD and μ-Raman spectroscopy) were used to evaluate the performance of TSA coatings in the presence of defects in artificial seawater. By using non-invasive techniques such as voltammetry around OCP (VAOCP, [21,22]) and EIS, corrosion mechanisms and service life of TSA coatings with defects can be evaluated without causing extensive damage to the samples, which enhances the understanding of corrosion protection performance of TSA coatings in marine environments.

2. Materials and methods

2.1. Materials and sample preparation

TSA coatings were deposited by Twin Wire Arc Thermal Spray (TWAS) following the optimised parameters shown in Table 1. The process consists of charging two wires (one positive, one negative) to create an electric arc that melts the wires. A compressed air stream directs the aluminium particles in a molten or semi molten phase towards the steel substrate. Prior to the thermal spray process, substrates (40 × 40 × 6 mm) were prepared with a standard of cleanliness of Sa 2.5 (ISO8501−1). This was achieved by grit blasting with angular alumina (NK36 type, 0.250−0.297 mm) and 100 psi air pressure. Commercially pure aluminium (1050 alloy, 99.5 wt% Al) in wire form (2.3 mm Ø) was used as the consumable and carbon steel (Table 2) was used as the substrate. The TSA coatings obtained have a rough surface (R_a17 ± 2 μm) and a 5–10 % porosity. The roughness of the TSA coatings was measured by 3D profilometry (Alicona InfiniteFocusSL and Alicona Imaging GmbH Software, Bruker Alicona, Austria). Porosity of the coatings was determined by image analysis (ImageJ Software), using threshold colour tool on SEM images of cross sections. These measurements were repeated three times.

In order to study the corrosion behaviour of the TSA coatings, three types of samples were prepared for electrochemical tests: a) TSA coating (named TSA), b) TSA coating with a nominal 5 % of surface area defect (named TSA5), and c) a bi-electrode recreating the TSA coating with a nominal 5 % of surface area defect where TSA and steel parts are isolated (named TSA5B). The size of the defect on these samples was chosen to represent damage of coatings in transportation/installation of structures and possible deterioration during service. Fig. 1 shows images of the three different types of TSA samples prepared.

For TSA5 samples, a circular holiday (artificial defect) of 10 mm Ø and 0.8 mm depth was machined at the centre of the TSA coated sample with a flat (slot) drill. Threaded rods were inserted on one side of the samples to be used as the electrical connection with the potentiostat. A Type 45 stopping-off lacquer (MacDermid plc, UK) was applied on all sides of the sample except from the one coated with TSA. Bi-electrode samples (TSA5B) were manufactured in collaboration with the Laboratoire des Sciences de l'Ingénieur pour l'Environnement (LaSIE) at La

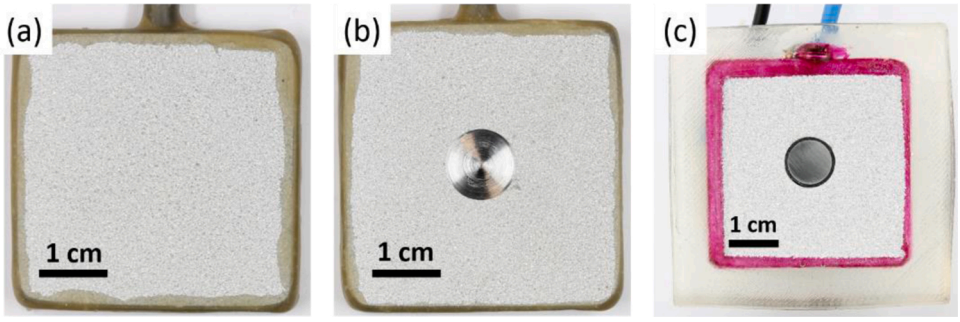

Fig. 1. TSA samples prepared for corrosion tests; (a) TSA sample, (b) TSA5 sample and (c) TSA5B sample.

Rochelle (France). First, a hole of 10 mm Ø was machined into the centre of the steel substrates. Second, TSA coating was applied following previously described procedure. Then, small carbon steel discs (same grade as the substrate) of 9 mm Ø and 6 mm thickness were manufactured in order to fit the hole in the TSA samples. The curved tubular sections of these discs were coated with 0.5 mm thick layer of resin to avoid electrical contact between the steel disc and the TSA sample. The surface of the steel discs was ground to P1200 finish with silicon carbide (SiC) abrasive paper. Finally, the discs were inserted in the holes of TSA samples. Electrical connections for each part of the sample were created by welding copper wire; one to the side of the TSA sample and one to the back of the steel disc. The bi-electrodes were then mounted in epoxy resin to expose a known area of the surface.

For cross-section examination, samples were cold mounted with Epofix resin (Struers Inc, Cleveland, USA) and cut through the middle with a vertical abrasive cutting saw (Buehler Abrasmatic 300, Illinois, USA). The surface was then ground with SiC abrasive papers going from P120 to P2500, and polished successively with 3 μm, 1 μm and 0.25 μm diamond paste.

2.2. Electrochemical corrosion tests

Corrosion performance of TSA coatings in fully immersed conditions was evaluated by several electrochemical techniques. All measurements were carried out with in-house artificial seawater following ASTM D1141 as electrolyte, in stagnant conditions and at ambient temperature (18 ± 3 °C). A three-electrode configuration cell was used with the TSA samples as working electrodes, a Pt/Ti wire or mesh as counter electrode and an Ag/AgCl (sat. KCl) as a reference electrode. Therefore, all potentials presented in this paper are with respect to the Ag/AgCl (Sat. KCl) electrode (E_{ref} = +0.199 V vs SHE, i.e.−0.045 V vs SCE at 20 °C). For electrochemical measurements, two different potentiostasts/galvanostasts were used: a Biologic VMP3 with an EC-Lab software for analysis (Bio-Logic Science Instruments); and a Gamry Interface1000 with Gamry Analyst software for analysis (Gamry Instruments). The reproducibility of the results was checked by performing each experiment twice.

Electrochemical characterization of TSA, TSA5 and steel was carried out by potentiodynamic polarization, after 24 h of immersion in artificial seawater in order to reach stable open circuit potential (OCP) values. The potential was swept from OCP-500 mV to OCP + 500 mV, at a 0.2 mV s^{-1} scan rate (dE/dt). Open circuit potential (OCP) was also recorded every 1 h for 30 days to monitor the electrochemical behaviour of samples in artificial seawater.

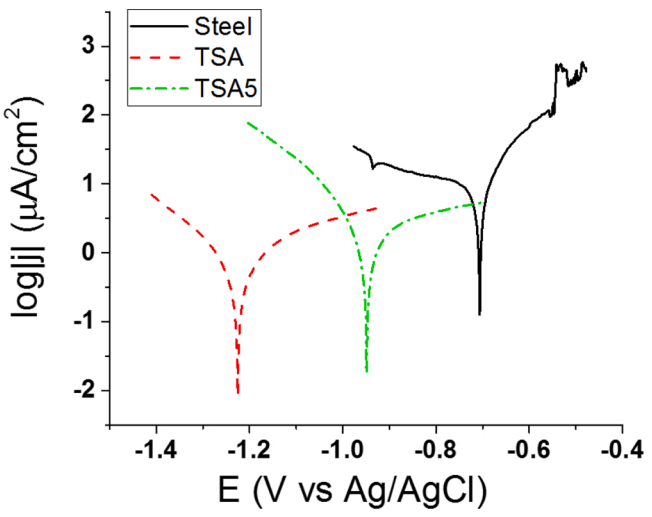

Fig. 2. Polarization curves Steel, TSA and TSA5 after 24 h immersion in artificial seawater.

In order to obtain information on the processes occurring around OCP without altering the electrodes' surface, voltammetry around OCP (VAOCP) was used. This method is called VAOCP to distinguish from "common" voltammetry performed on a larger potential range. It was initially proposed [21,22] as an alternative non-destructive approach to monitor the evolution of corrosion processes, in combination with EIS. To obtain accurate and reliable information, the voltammograms, obtained on a short range (typically ±50 to ±70 mV) of potential around OCP, must be computer-fitted using electrochemical kinetic laws. The method is not consequently restricted to the (rare) cases where both anodic and cathodic reactions obey Tafel law. This is a crucial point because the reduction of dissolved oxygen, for instance, is not generally controlled by charge transfer. VAOCP may however be unreliable in some cases. For example, a given voltammogram may be adequately fitted in many ways leading to an error in the calculated corrosion current density [21]. For this reason, the method must be used with care and coupled with other electrochemical methods, such as EIS.

Measurements were carried out after 10, 20 and 30 days of exposure to the electrolyte. Polarization curves were recorded at dE/dt = 0.2 mV s^{-1}, sweeping the potential from OCP to OCP + 50 mV, then to OCP -50 mV and finishing back at OCP. This procedure allows estimating the amplitude of the perturbation induced by the polarization at the metal/electrolyte interface. In most cases, this perturbation induces a difference between positive-going and negative-going scans, like a hysteresis effect. If this effect is kept small, the polarization curve can be reliably used, whatever the scan direction. To facilitate the comparison between the various experiments, the negative-going part of the scan (from OCP + 50 mV down to OCP – 50 mV) was considered in each case for the computer fitting analysis.

Electrochemical impedance spectroscopy (EIS) measurements of TSA and TSA5 samples were recorded at OCP. The frequency range for each scan was from 100 kHz to 20 mHz, with a 10 mV peak-to-peak sinusoidal voltage and 10 points per decade. The EC-Lab software (Bio-Logic) was used to fit the impedance spectra collected using electrical equivalent circuits. The deviation between experimental data and calculated spectrum was evaluated based on the chi-squared values (χ^2). Therefore, after several fitting processes, the circuits providing the smallest values of χ^2 where chosen.

The bi-electrodes were used to study independently (via EIS) the electrochemical processes taking place on the TSA coated part (mainly anodic) and on the steel part/defect (mainly cathodic). The evolution of the OCP of the whole electrode was monitored over time. It must be noted here that this OCP is a mixed potential, intermediate between the potential of the steel part and the potential of the TSA coated part. To perform EIS measurements on each part of the bi-electrode, the two parts must be disconnected. Consequently, in order to minimize the impact on the system of this disconnection, both parts of the bi-electrode were maintained at the last measured value of the mixed potential during this period. Prior to the EIS scan, the part of the electrode to be measured was held potentiostatically at the mixed potential for 300 s. Then, potentiostatic EIS was carried out at the mixed potential as described above for TSA and TSA5 samples. Finally, during the potentiostatic polarization of the steel part applied for 300 s before each EIS experiment, the current was monitored. It corresponds to the current required for the cathodic protection of the steel part/defect, which is provided by the dissolution of the TSA when both parts of the electrode are connected.

2.3. Characterization of corrosion products

Corrosion products formed on the specimens after exposure to artificial seawater were characterised by Scanning Electron Microscopy and Energy Dispersive X-ray (SEM-EDX) using an EVO LS15 SEM/EDX (Zeiss, Obekochen, Germany). Images were obtained with a 20 kV voltage, 4.5 μm spot size, 8.5 mm working distance and backscattered electron detector. Samples were also analysed by μ-Raman spectroscopy,

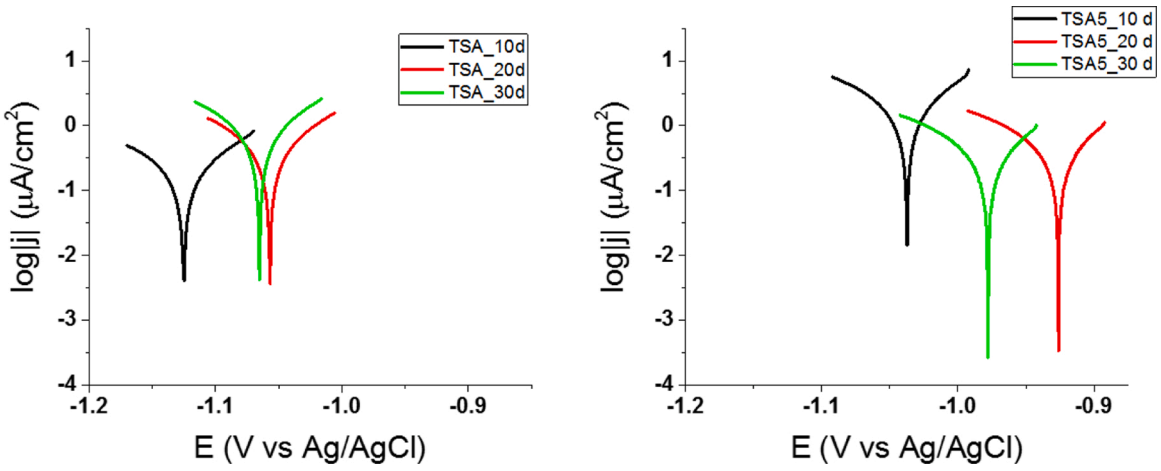

Fig. 3. VAOCP curves of TSA and TSA5 over time of immersion in artificial seawater.

using a Jobin–Yvon Raman spectrometer (LabRAM-HR) set up with an Olympus- BX41 microscope and a Peltier-based cooled charge coupled device (CCD) detector. Collection of the μ-Raman spectra was carried out at room temperature and with excitation provided by a He-Ne laser (632.8 nm). The power of the laser was reduced between 1% and 25 % to prevent excessive heating of corrosion deposits. Finally, X-ray diffraction (XRD) analysis was performed. The equipment used was an Inel EQUINOX 6000 diffractometer (Thermo Fisher Scientific, Waltham, MA) with a CPS 590 curved detector that can simultaneously detect the diffracted photons on a 2θ range of 90°. Acquisition parameters used were a constant angle of incidence of 5°, using the Co-Kα radiation (λ =0.17903 nm) during 45 min. The different phases were identified using the ICDD-JCPDS database.

3. Results and discussion

3.1. Electrochemical characterization of TSA coated steel

Initial characterization of the materials was carried out by potentiodynamic polarization after 24 h immersion in artificial seawater. Fig. 2 shows the polarization curves of uncoated steel, TSA-coated steel and TSA-coated steel with a 5 % of surface area defect. The three curves are characterised by drastically different corrosion potential (E_{corr}) values. Thermally sprayed sample TSA presents an E_{corr} value typical of Al, i.e.−1.2 V vs Ag/AgCl, whereas the E_{corr} value for steel is much higher, about -0.7 V vs Ag/AgCl. Finally, the E_{corr} value of TSA5 is between the two above, at about -0.9 V vs Ag/AgCl. The potential of TSA5 is a mixed potential, intermediate between that of Al (the TSA coated part being mainly an anodic zone) and that of steel (the defect being a cathodic zone protected by the galvanic effect).

Steel is an active metal in seawater, which leads to a sharp increase of the current density with the potential in the anodic region. On both TSA samples, the slope of the curve in the anodic region is much smaller, which indicates that Al tends to passivate, i.e. the dissolution of the metal only takes place at defects of the passive layer. It should be noted that the breakdown of the passive film from pitting corrosion is not observed here due to the limited range of the potentiodynamic sweep. At higher potential values, the chloride ions present in seawater react with the aluminium oxide film, which results in a rapid increase of current values. When wider limits of potentiodynamic scans are applied for TSA coatings in chloride solutions (below -1.45 V and above -0.75 V vs Ag/AgCl), the film breakdown is observed as it has been reported in literature [23–25].

The corrosion current density j_{corr} is similar for TSA and TSA5 samples, while it is higher for steel that does not tend to passivate at all in seawater. The respective values of j_{corr} for TSA and TSA5, and their evolution with time are reported in detail in the "VAOCP monitoring" section.

3.2. VAOCP monitoring

In order to understand the corrosion protection offered to steel by TSA coatings, it is important to obtain information about the anodic and cathodic processes taking place. VAOCP was used together with EIS as a complementary method to monitor the evolution over time of these processes.

Polarization curves of TSA and TSA5 samples were obtained after 10, 20 and 30 days of exposure to artificial seawater (Fig. 3). In both cases, ennoblement of the E_{corr} values between 10 and 30 days of immersion can be observed. In contrast, the evolution of the corrosion current density over time seems different. For the TSA sample, j_{corr} increases between 10 and 30 days. For the TSA5 sample, j_{corr} decreases. This point can be confirmed, and the evolutions quantified, via the modelling of the polarization curves.

To model these curves, it was assumed that the anodic reaction followed Tafel law. For the cathodic reaction, mainly associated with O_2 reduction, a kinetic at least partially controlled by diffusion could have been expected. However, the polarization curves show that the cathodic reaction is not totally controlled by diffusion as revealed by the shape of the cathodic branch. An activation control was even suspected and a first modelling was attempted using the Butler-Volmer equation for both anodic and cathodic reactions. The experimental polarization curves could not be correctly fitted with this first model, which indicated that the cathodic reaction was under mixed activation-diffusion control. The Koutecky-Levich equation was then used to model the cathodic reaction rate, as described in previous works [21,22]. The anodic (j_a) and cathodic (j_c) current densities were then expressed by Eq.s 4 and 5 respectively:

$$j_a = j_{corr}\, e^{\beta_a (E - E_{corr})} \tag{4}$$

$$j_c = \frac{1}{\frac{1}{j_{lim}} - e^{-\beta_c (E - E_{corr})} \cdot \left(\frac{1}{j_{corr}} + \frac{1}{j_{lim}} \right)} \tag{5}$$

Here, j_{lim} represents the limiting current density associated with O_2 diffusion and β_a and β_c are the anodic and cathodic Tafel coefficients (V^{-1}) respectively. Combining these, the polarization curve j vs E can be modelled with the following experimental function:

$$j = j_a + j_c = j_{corr}\, e^{\beta_a (E - E_{corr})} + \frac{1}{\frac{1}{j_{lim}} - e^{-\beta_c (E - E_{corr})} \cdot \left(\frac{1}{j_{corr}} + \frac{1}{j_{lim}} \right)} \tag{6}$$

Table 3
VAOCP fitting results of TSA and TSA5 samples over time of immersion in artificial seawater. The error for j_{cor} and b_a is estimated at ±20 %; while that on E_{corr} is ±1 mV. The values for b_c and j_{lim} are in brackets as the error is high (about ±50 %).

	b_a (mV decade^{-1})	b_c (mV decade^{-1})	E_{corr} (V)	j_{corr} (μA/cm^2)	j_{lim} (μA/cm^2)
TSA_10d	92	(60 ± 30)	−1.12	0.2	(-0.8 ± 0.4)
TSA_20d	115	(110 ± 55)	−1.06	0.7	(-4 ± 2)
TSA_30d	115	(110 ± 55)	−1.07	1.2	(-8 ± 4)
TSA5_10d	115	(110 ± 55)	−1.04	2.9	(-20 ± 10)
TSA5_20d	85	(80 ± 40)	−0.94	0.5	(-3 ± 1.5)
TSA5_30d	92	(90 ± 45)	−0.99	0.5	(-6 ± 3)

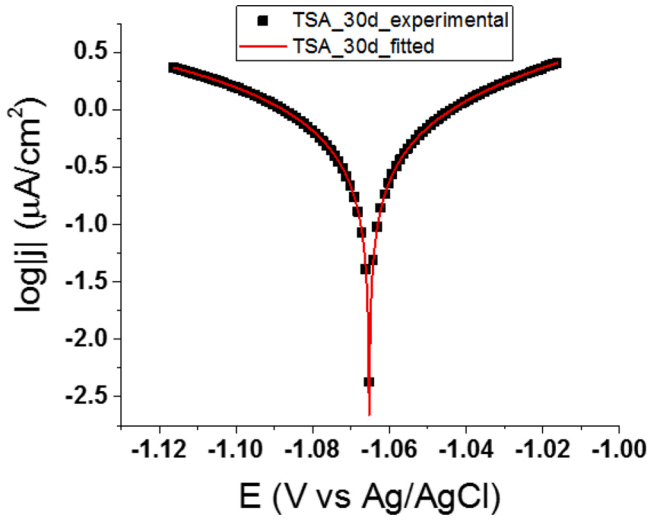

Fig. 4. VAOCP fitting of TSA sample immersed in artificial seawater for 30 days.

The corrosion potential (E_{corr}) was directly obtained from the log|j| vs. E curve. Then, the Tafel coefficients β_a and β_c, corrosion current density (j_{corr}) and limiting cathodic current density (j_{lim}) were calculated by computer fitting. The obtained Tafel coefficients were finally converted to Tafel slopes ($b_{a,c} = \ln(10)/\beta_{a,c}$) for comparison with literature data. The values obtained from the simulations are shown in Table 3. The accuracy of the electrochemical parameters determined for the cathodic reaction is quite low (~50 %), because various (β_c, j_{lim}) couples were observed to lead to a correct fitting of the experimental data, as already noted [21]. For this reason, the values obtained for these parameters are not discussed.

An example of the obtained results is given in Fig. 4, where a computed curve is compared with an experimental curve. It can be seen that the chosen electrochemical laws allowed obtaining excellent computer fittings. This confirms that the cathodic reaction is partially controlled by diffusion. For the TSA sample, O_2 diffusion would take place through the corrosion product layer that progressively covers the active parts of the TSA coating. For the TSA5 sample, the cathodic reaction mainly takes place on the steel surface, where O_2 would diffuse through the calcareous deposit.

For the anodic reaction, a charge transfer mechanism was considered, which proved satisfactory. However, a diffusional process may be involved ("apparent" Tafel behaviour) as observed for instance for copper [26]. For both TSA and TSA5 samples, the anodic Tafel slopes b_a values are approximately constant and within the 105 ± 30 mV decade^{-1} range. These values are in agreement with those previously published for TSA [27,28].

The determination of j_{corr} confirms that opposite trends are observed for each sample. The sample without defect presents an increase in the corrosion current density. This means that as the system evolves with time, the dissolution rate of Al increases. For the TSA5 sample however, the corrosion current density decreases over time. This last result can be attributed to to the formation of a protective layer of corrosion products. These corrosion products, forming more rapidly on TSA5 due to the galvanic coupling with the steel in the defect, have a beneficial effect and decrease the corrosion rate of the active parts of the coating (i.e. at the defects of the passive layer). For the TSA without defect, the increase of j_{corr} indicates that the increasing number and size of defects present in the passive layer, due to the exposure to seawater, are not counterbalanced by the slower formation of the protective corrosion products. The increase of $|j_{lim}|$ in the case of the TSA sample (Table 3) may then be attributed to an increase of the active area. Conversely, the decrease of $|j_{lim}|$ in the case of the TSA5 sample illustrates the beneficial effect of the protective corrosion product layer.

3.3. EIS study of corrosion of TSA in seawater

Corrosion performance of TSA coatings was also evaluated by EIS measurements. Fig. 5 shows the Nyquist and Bode diagrams of the three samples under study. EIS data was recorded at different immersion times in artificial seawater at room temperature. For all measurements, the application of the Kramers-Kronig relationships revealed that the impedance values measured at low frequencies (below 30 mHz) were not reliable, therefore those were neglected for the modelling of the curves. The points represent experimental data, and the solid lines the fitting curves for each spectrum.

Fig. 6 shows the electrical equivalent circuits (EEC) used to fit the various experimental EIS data. It must be noted that the CPE/R elements used on the EEC of Fig. 6(a) and (b) correspond to the TSA-solution interface. In all cases, R_s represents the solution resistance, R_1 is associated with the charge transfer resistance of the coating and a constant phase element (CPE) represents the double layer capacitance at the electrolyte/TSA coating interface. A CPE is used instead of an ideal capacitance to take into account the effects due to inhomogeneity, porosity, roughness, and other non-ideal dielectric properties of the electrode [29]. The deviation from ideal behaviour is expressed by the CPE coefficient n; $n = 1$ for a true capacitor, $1 < n < 0.7$ for a CPE and $n = 0.5$ for a diffusion element. Fig. 6 (a) represents the simple Randles circuit, used to fit data of a coating or corroding material. Fig. 6 (b) includes a W_d diffusional element, which represents a bounded diffusion phenomenon (finite-length diffusion for a planar electrode) through the corrosion product layer and/or the calcareous deposit on steel (defect). Finally, Fig. 6 (c) shows an EEC with the solution resistance (R_s) and two diffusion elements (W_{d1} and Wd_2). This EEC was retained because it gave a significantly improved goodness-of-fit, when compared with a circuit composed of only one diffusion element. The possible meaning of these two elements is carefully discussed later, as this unusual model still remains an assumption. Tables 4 and 5show the values of the circuit parameters obtained from the fitting method.

The Nyquist diagrams of the TSA sample present one semicircle from 10–30 d of exposure. For 10 d and 20 d, the EIS data do not show any hint of a diffusion process. Only one single capacitive loop is observed and the EEC of Fig. 6(a) was used accordingly, which resulted in a satisfactory goodness-of-fit. This result shows that the process is not controlled by diffusion at that time, i.e. is not controlled by the cathodic process. It is then controlled by the anodic process, in this case associated with the properties of the imperfect passive layer that covers the TSA surface. The dissolution of Al only takes place at the defects of this passive layer and the anodic area is kept small. The number and size of defects then control the kinetics of the corrosion because a sufficient amount of dissolved O_2 is always available at the vicinity of the defects. After 30 days of exposure, the phase angle however decreases to 64° and a shoulder appears, indicating a diffusion process [27,29]. The EEC used

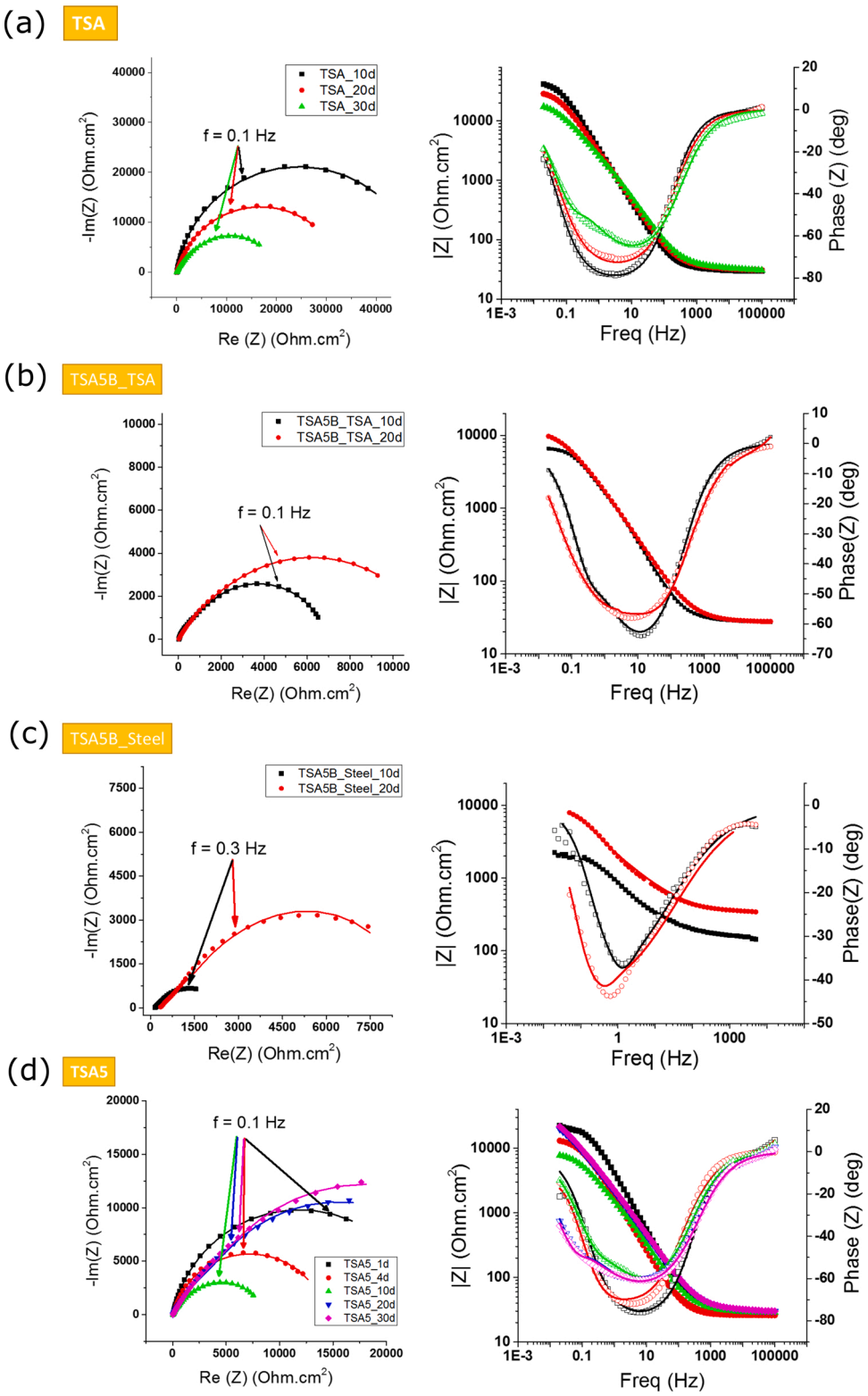

Fig. 5. EIS data representation over time as Nyquist and Bode plots of three samples exposed to seawater. (a) TSA coating with no defect (TSA), (b) TSA part of TSA5B bi-electrode (TSA5B_TSA), (c) steel part of TSA5B bi-electrode (TSA5B_steel) and (d) TSA coating with a 5 % of surface area defect (TSA5).

to fit the data collected after 30 d of exposure then included a W_d bounded diffusion element (Fig. 6 (b)).

The charge transfer resistance (R_1) values obtained decrease over-time. This result is fully consistent with the evolution over time observed for j_{corr} via VAOCP measurements: j_{corr} increases from 0.2 μA/cm^2 to 1.2 μA/cm^2 (Table 3) while R_1 decreases from 49 kΩ cm^2 to 6.2 kΩ cm^2 (Table 4). This confirms that the corrosion rate of TSA increases over time. The dissolution of the air-formed oxide layer on top of the TSA results in an increase of surface area. As this layer gets progressively damaged, the number and size of its defects increase, leading to an increase of the dissolution rate of Al. However, at 30 days the influence of the corrosion products that form on the active parts of the coating

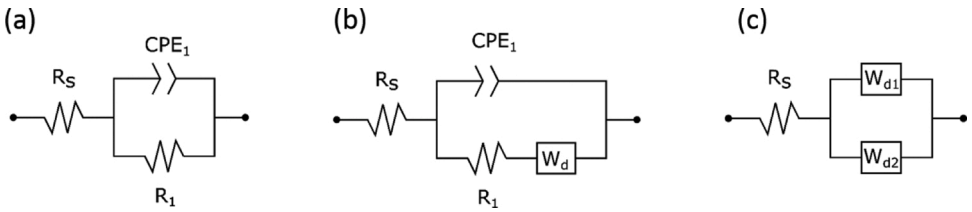

Fig. 6. EEC used to fit EIS data.

Table 4
Fitted values of TSA samples.

Impedance data fitting results of TSA samples immersed in artificial seawater at different times							
Material	Time of exposure (d)	R_s (Ω cm^2)	n	R_1 (Ω cm^2)	R_d (Ω cm^2)	t_d (s)	CPE$_1$/Q (F cm^{-2} s^{n-1})
TSA	10	30	0.91	49,000	–	–	5.7×10^{-5}
TSA	20	33	0.84	34,000	–	–	6.9×10^{-5}
TSA	30	32	0.80	6200	1300	3.2	7.0×10^{-5}
TSA5B_TSA	10	28	0.81	2700	380	1.2	1.0×10^{-4}
TSA5B_TSA	20	28	0.71	8700	310	2.2	1.5×10^{-4}
TSA5	1	2	0.88	24,000	–	–	4.6×10^{-5}
TSA5	4	2	0.85	14,000	–	–	1.2×10^{-4}
TSA5	10	29	0.75	4100	370	1.3	1.4×10^{-4}
TSA5	20	31	0.75	8800	1600	6.9	1.0×10^{-4}
TSA5	30	31	0.74	11,000	1900	7.4	10×10^{-5}

Table 5
Fitted values of EIS data of steel part of TSA5B bi-electrode.

Impedance data fitting results of steel electrode immersed in artificial seawater at different times						
Material	Time of exposure (d)	R_s (Ω cm^2)	R_{d1} (Ω cm^2)	t_{d1} (s)	R_{d2} (Ω cm^2)	t_{d2} (s)
TSA5B_Steel	10d	150	3400	0.6	15,500	4.0
TSA5B_Steel	20d	310	2100	1.8	46,000	11

become significant. The diffusion element in the EEC shows that, at 30 d, these corrosion products hinder the transport of oxygen.

It must finally be noted that the fitting of the VAOCP polarization curves for TSA samples implied in any case to use a mixed activation-diffusion controlled kinetics for the cathodic reaction. However, voltammetry investigates a wider potential range than EIS. This means that at 10 and 20 d, the cathodic reaction was controlled by charge transfer at OCP but was under mixed control at the lower potentials investigated through voltammetry. Actually, a further decrease of potential (lower than OCP-50 mV) could finally lead to the diffusion plateau where O_2 reduction is entirely controlled by diffusion.

Moving onto the sample formed by the separated TSA and steel electrodes and looking into the TSA coated part (TSA5B_TSA), the Nyquist diagrams present one depressed semicircle at middle-low frequencies, with a 45° slope at high frequencies. In addition, the diameter of the loop increases with time, which means that the corrosion resistance increases over time [11,27,29]. Here, the EEC used to fit the data is the Randles circuit with a W_d bounded diffusion element also for 10 and 20 d of exposure (Fig. 6 (b)). It is first observed that the charge transfer resistance (R_1) values increase from 2.7 kΩ cm^2 to 8.6 kΩ cm^2 in this case. The phase maximum on the Bode plot decreases from 64° at 10 d to 58° at 20 d. This is more likely due to the formation of a corrosion product layer on the active areas of the coating, as a result of the reaction with artificial seawater [11,27]. This layer hinders O_2 diffusion. In addition, the exposure time needed to observe the shoulder on the phase plot as a result of the diffusion process is reduced from 30 d for the TSA sample to 20 d for the TSA5B_TSA one. Comparing EIS data of TSA and TSA5B_TSA, different trends are observed on the initial days of exposure. As R_1 decreases over time for the former one, it increases for the latter. On the Bode plots, phase angle after 20 d of exposure is around 70° for TSA, however for TSA5B_TSA it is 58° after the same exposure time. This reflects once again how when there is bare steel exposed to the solution, the formation of the corrosion product layer on the TSA is accelerated. Consequently, its beneficial effects appear sooner.

Looking at the steel part of the bi-electrode (TSA5B_Steel), the Nyquist diagrams show one semicircle. Actually, there are two loops on the Nyquist plots but the loop at high frequency is very small and incomplete and cannot be fitted reliably. Therefore, it was removed for the fitting and it is not shown on the graph. This explains why the R_s values are large, equal to 146 and 308 Ω cm^2, values that may correspond to the omitted capacitive loop present at high frequency [14,15].

The diameter of the main semicircle increases over time. The impedance values obtained here are attributed to the formation of the calcareous deposits on top of the steel surface as a consequence of the cathodic reaction. Looking at the Bode plots, the phase angle presents an asymmetrical shape with very low values below 50° (not typical of CPE), and the n values determined graphically from experimental data (imaginary part of the impedance vs frequency) are around 0.5. This reveals unambiguously a diffusion process. In this case, the cathodic reaction, i.e. O_2 reduction, is diffusion controlled.

The EEC consequently used to fit the data of the steel part of the bi-electrode is represented in Fig. 6 (c) and reflects the importance of diffusion. Only two diffusion elements (plus R_s) were used and so they more likely include or mask the charge transfer resistance and the double layer capacitance. The use of the two W_d elements (W_{d1} and W_{d2}) could mean the diffusion of different species through the deposits on top of the steel, or diffusion of O_2 through different deposits or zones of the deposit having different properties with respect to oxygen diffusion [14,15]. Actually, SEM observations (see description later in the paper) indeed revealed the presence of two kinds of zones in the calcareous deposit. It can be seen in Table 5 that both t_{d1} and t_{d2} increase with time. R_{d2} also increases while conversely R_{d1} decreases with time. Actually, after 20 days, the R_{d2}:R_{d1} ratio is about 22, which shows that one of the diffusion paths (#2) plays a main role in the process. In the expression of the diffusion impedance, R_d is a scaling factor that depends on the kinetics of the interfacial reaction and the bulk concentration of the electroactive species. The increase of R_{d2} may then express the decrease of the O_2 reduction rate on the steel surface. According to [30,31], the diffusion time constant t_d is link to the thickness δ_f of the layer through which O_2 diffuses via the equation:

$$t_d = \frac{\delta_f^2}{D_f} \tag{7}$$

where D_f is the diffusion coefficient of oxygen through the layer. The

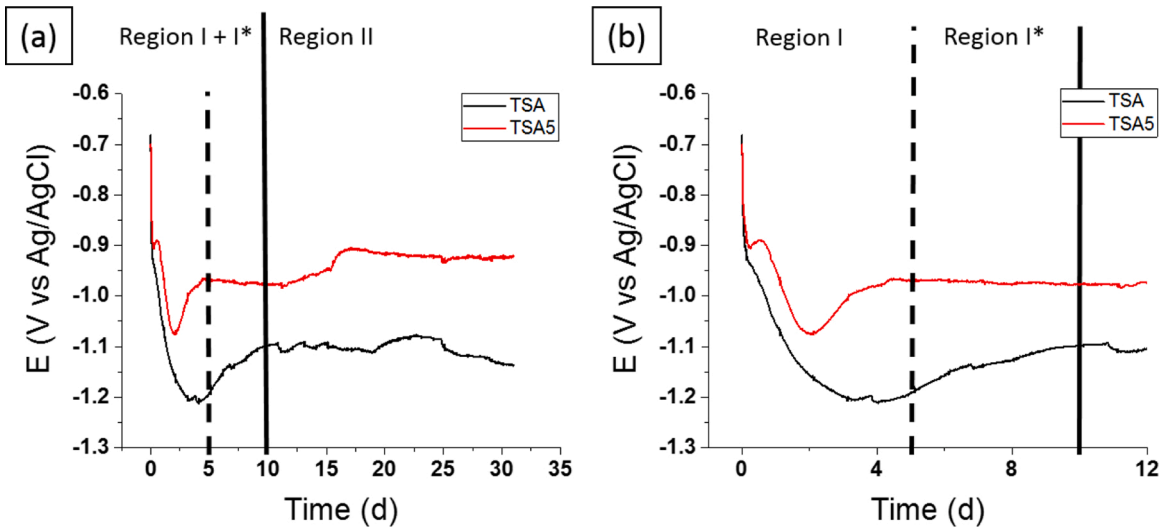

Fig. 7. OCP values of TSA and TSA5 samples exposed to artificial seawater for 30 days.

increase of both t_{d1} and t_{d2} with time shows that both kinds of layers (in the calcareous deposit) are getting thicker with time, and the larger value of t_{d2} more likely indicates that the layer #2 is thicker than the layer #1. Even though the EEC used here is unusual, as a single diffusion element would have been expected, the information it provides is consistent with those given by surface characterization (see following section), and illustrate the beneficial effect of the calcareous deposit. The deposit hinders more and more efficiently O_2 diffusion and restricts the cathodic reaction rate at the steel surface in the defect. This is clearly illustrated by the chronoamperometric measurements performed prior to the EIS measurements: after 10 days, the current demand was equal to j_{CP} = -26 ± 2 μA/cm^{-2}. After 20 days, it was much smaller (in absolute value), and equal to j_{CP} = -5 ± 0.5 μA/cm^{-2}.

The Nyquist diagrams of TSA5 sample are also shown in Fig. 5. In this case, measurements were achieved during the initial 4 days as well in order to corroborate the assumption based on the role of the corrosion products forming when the TSA coating is immersed in seawater. Here, from 1 to 4 days the *Z* values decrease as observed for the TSA sample. Therefore, the EEC used to fit the data of TSA5 sample exposed up to 4 days did not include the diffusion element (Fig. 6 (a)). For longer exposure times, the expansion of the semicircle and the increase on the impedance modulus showcase a better corrosion resistance with immersion time. This correlates to the behaviour observed for the TSA part of the TSA5B bi-electrode. Over time, due to the coupling with the exposed steel, the corrosion products form quicker. Polarizing demand from steel accelerates Al dissolution and therefore promotes the formation of these products that occurs in this case within the 10 first days. Once calcareous deposits are stable on top of the steel substrate, cathodic reaction slows down and therefore polarizing demand decreases. From 20 d after immersion, there are no significant changes observed in the corrosion resistance of the coating. As a result of formation of deposits on both the coating and the steel substrate surface, impedance modulus changes only slightly. From 10–30 d of exposure, the Randles circuit (Fig. 6 (b)) was used to fit the data and the charge transfer resistance (R_1) values increase from 4.1 kΩ cm^2 to 11 kΩ cm^2, with R_d also increasing from 370 to 1900 Ω cm^2. Once again, the EIS results are consistent with the VAOCP analysis: j_{corr} was observed to decrease from 2.9 μA/cm^2 to 0.5 μA/cm^2 (Table 3). This confirms that the corrosion rate of TSA5 samples decreases with time (while that of TSA sample increases with time).

Comparing these values to the TSA part of the bi-electrode, they present similar values and tendencies. On the Bode plots, phase maximum decreases from 80° after 1 day of immersion to 60° after 10 days of immersion. Furthermore, the diffusion shoulder on the phase angle data appears after 10 days of exposure. The presence of diffusion corroborates the influence of a barrier for O_2; calcareous deposits on the steel, and corrosion product layer on the TSA coating. It should be noted that the species involved in the diffusion process cannot be measured. As the cathodic reaction is the limiting one, it is assumed that the diffusion would correspond to the movement of O_2 through calcareous deposit/corrosion product layer. However, Al ions from the anodic reaction would also have to diffuse through the TSA corrosion product layer.

3.4. OCP measurements

The OCP measurements can now be presented and discussed in light of VAOCP and EIS results. Fig. 7 shows the curves obtained over a 30 day immersion in artificial seawater for a TSA sample without defect (TSA) and with a 5 % of surface area defect (TSA5) exposing the steel substrate.

For both samples, two regions can be observed in the OCP graphs:

- Region I + I*: an initial drop in potential is observed for both samples, followed by an increase towards less negative values until stabilization is reached around -1.0 V for the TSA5 sample and around -1.1 V for the TSA sample. Looking at the data collected over the initial 12 day period, the transition can be observed from region I to region II at two different points in time for each sample. Region I extends from 0 to 5 days of exposure and it corresponds to the region where sample TSA5 presents the initial drop in OCP. Region I* extends from 0 to 10 days of exposure, and it corresponds to the region where sample TSA presents the initial drop of OCP.
- Region II: potential values on this region present small variations on both samples, around -1.0 V for the TSA5 sample, and around -1.1 V for the TSA sample.

The initial decrease towards more negative OCP values at the beginning of the experiments shown in region I + I* can be attributed to the degradation of the air-formed oxide layer of TSA (increasing number and size of defects), which increases the active surface area of the aluminium. The following increase in potential towards more positive values is more likely a consequence of the formation of solid corrosion products on the active parts of the TSA surface. After several days of exposure, the formation of these corrosion products covers the defects of the coating, which considerably decreases the active surface area of the TSA coating. These trends have been also been observed on previous studies reported with TSA coatings [10,19,32]. However, the transition from region I to region II occurs at different points in time depending on the presence or absence of a defect on the TSA coating. For the TSA

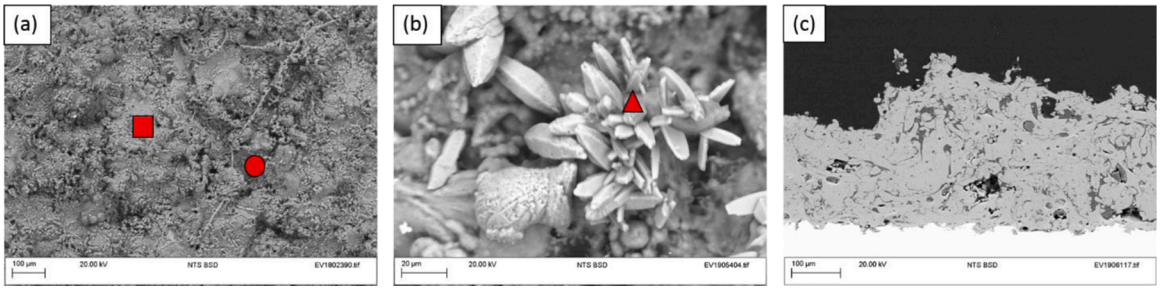

Fig. 8. SEM images of TSA coating; (a), (b) top view and (c) cross section.

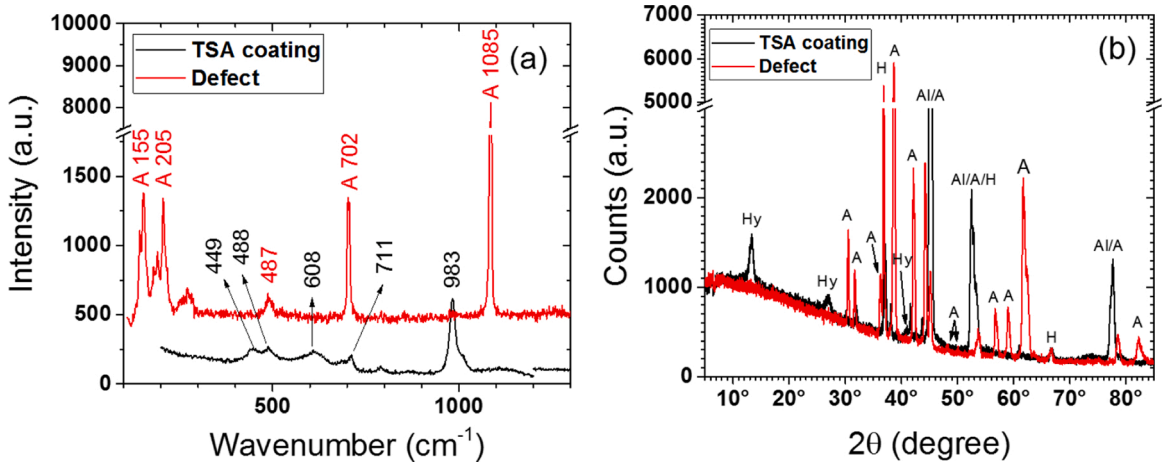

Fig. 9. Raman spectrum (a) and XRD pattern (b) of the coating area of the TSA5 sample immersed in seawater for 30 days. A: aragonite; Hy: hydrotalcite; A: aluminium; H: halite.

sample, stabilization of potential values requires at least 10 days of immersion in solution. For the TSA5 sample, stable potential values are observed after 5 days, that is, half the time of the TSA sample without an artificial defect on the coating. The presence of the defect accelerates the dissolution of Al and therefore, the formation of the corrosion products as well. On the TSA sample with a 5 % of surface area defect, the formation of the calcareous deposits on top of the exposed steel also occurs during the first few days of immersion. Due to the direct exposure of the steel to the solution, cathodic reaction is enhanced, and therefore the anodic reaction of dissolution of aluminium gets accelerated in comparison with the TSA without the defect. As a result, transition time from region I to region II is reduced for TSA samples with defects. It should be noted that formation of calcareous deposits is only possible in seawater (natural or artificial) that contains Ca^{2+}, Mg^{2+} and HCO_3^- ions. Therefore, in order to study behaviour of these samples in marine environments, electrochemical tests in simplified solutions such as 3.5 % NaCl are not relevant.

3.5. Characterization of corrosion products

After 30 days of exposure to artificial seawater, characterization of the corrosion products formed on top of all the samples previously described (TSA, TSA5 and TSA5B) was performed by SEM-EDX (Fig. 8), μ-Raman and XRD (Fig. 9). In addition, cross-sectional analysis of the samples was carried out in order to look at the structure of the coating after exposure and the deposits formed on top of the steel. Due to the similar nature of the samples in terms of materials (TSA coating on a steel substrate), same corrosion products were identified on all samples. Therefore, the data presented in this section corresponds to the analysis of the TSA coated steel substrate with a 5 % of surface area defect (TSA5).

Fig. 8 shows top view (a, b) and cross section (c) SEM images of the TSA coating from a TSA sample with a 5 % of surface area defect exposed to artificial seawater for 30 days. From these, the characteristic high roughness of the TSA coating can be observed, and two different phases where identified; light grey main phase covering most of the sample (■) and darker grey localised regions (●). In addition, small amounts of crystalline structures were found scattered on top of the light grey matrix (▲).

These two phases were observed on all samples under study, with no significant differences between samples with or without defects. After 30 days of exposure, all coatings are expected to show Al corrosion deposits on the surface even without artificially machined defects. From the cross section SEM image (Fig. 8 (c)), it can be observed how the pores of the coating are filled with aluminium corrosion products. Looking closely at the steel-TSA interface, it can also be noted that there are no signs of corrosion of the steel under the coating. Overall, there are no signs of major deterioration of the TSA coating over 30 days of exposure. However, over long periods of service time, these coatings are reduced in thickness as they provide cathodic protection to the steel substrate.

Further analysis of the samples by μ-Raman spectroscopy and XRD on the TSA coating revealed hydrotalcite deposits (Fig. 9). Due to the nature of the samples and the solution, a Mg-Al hydrotalcite is expected, with carbonates or sulphate ions in the interlayer. The presence of hydrotalcite containing CO_3^{2-} ions was corroborated by XRD pattern obtained from the top surface of the TSA coating (Fig. 9 (b)). Therefore, in our case it is the carbonated form that precipitated as identified in XRD pattern (Fig. 9 (b)), with sulphate ions adsorbed by hydrogen bonds.

The corrosion products could not be identified from the Al-O peaks. Due to the numerous possible combinations of vibrational frequencies, detailed assignment of individual bands is not possible. Thus, the 440 cm^{-1} to 790 cm^{-1} range of Raman frequencies is associated with Al-O

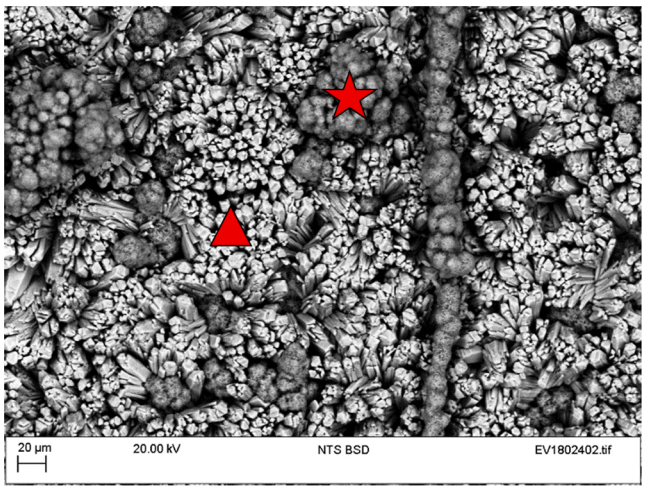

Fig. 10. Top view SEM image of defect area of TSA5 sample showing calcareous deposits.

vibrational frequencies based on literature [33–35]. On the XRD pattern (Fig. 9 (b)), there was no clear identification of aluminium oxides. The aluminium peaks identified correspond to the TSA coating (99.5 % Al). In addition, aragonite was found on top of the coating (Raman spectra of Fig. 9 (a) and XRD pattern of Fig. 9 (b)). This compound could form as a result of cathodic reaction taking place on the TSA coating, which could locally increase the pH at the TSA/solution interface and promotes precipitation of aragonite. Finally, halite (NaCl) has formed during the drying of the sample.

On top of the defect area of the TSA samples, where steel is directly exposed to artificial seawater, formation of calcareous deposits is well known [10,13,19]. These deposits then act as a physical barrier for further corrosion of the system as explained in previous sections. Fig. 10 shows a top view SEM image of the defect area where two distinct structures can be differentiated (▲,★). The presence of these two kinds of zones on the calcareous deposit may explain the two W_d diffusion elements used to interpret the impedance data of the steel part of the bi-electrode.

Raman and XRD (Fig. 9) analysis show that the Ca-rich structure (▲) corresponds to aragonite. However, brucite (★) was not observed with these techniques, more likely because brucite is mainly present under the aragonite layer as it can be observed in Fig. 11, focused on the sample/defect area. From the EDX maps of this figure, it can be appreciated how the Mg-containing deposits (brucite) formed predominantly under the Ca-rich layer of aragonite.

4. Conclusions

A combination of electrochemical and surface analysis of TSA coated steel samples with and without defects provided a new insight into the corrosion protection mechanism offered by these coatings in marine environments. It has been observed how a protective layer of Al corrosion products forms on top of TSA coatings under fully immersed

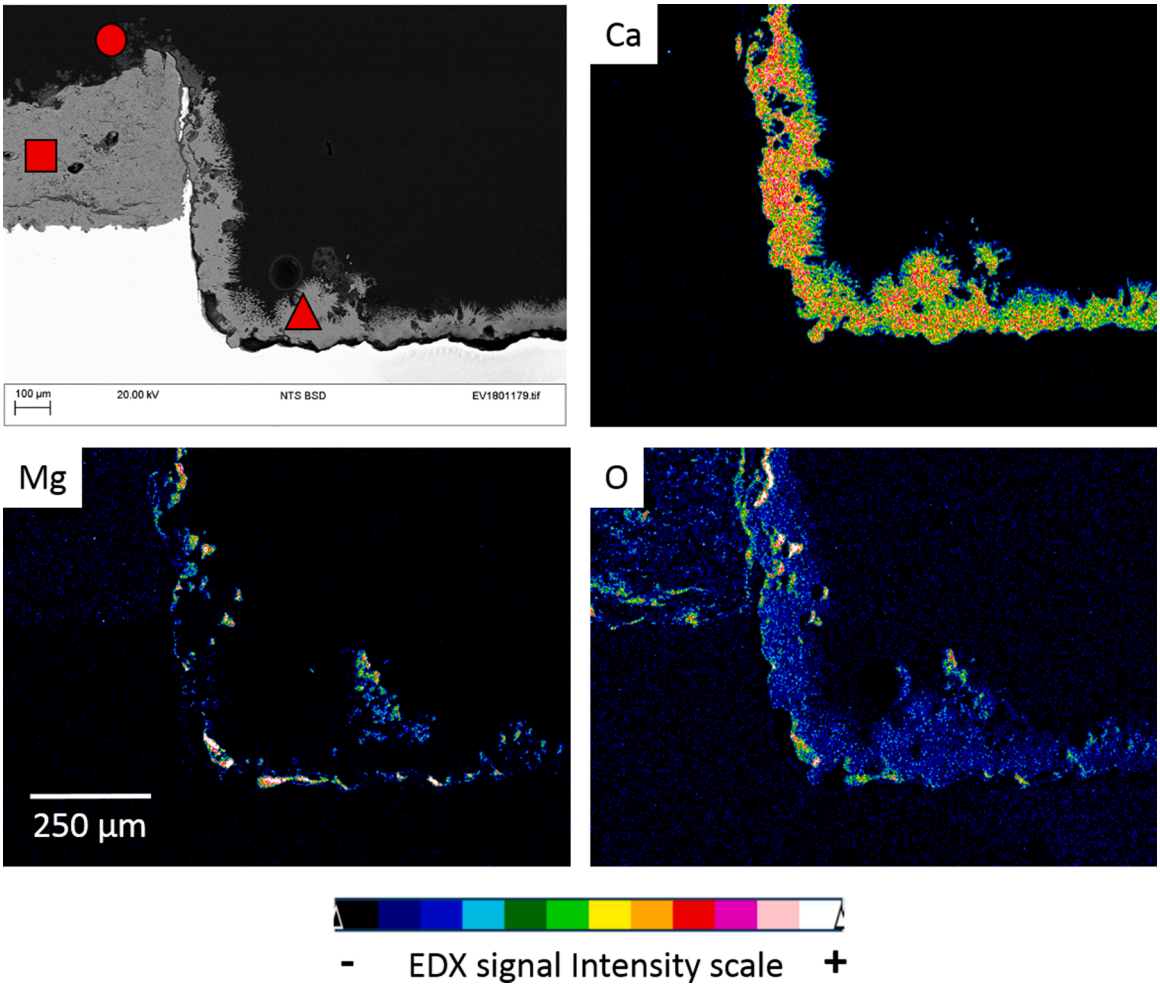

Fig. 11. SEM and EDX maps of TSA5 sample defect area.

conditions in artificial seawater. In addition, the formation of this layer is accelerated by the presence of defects on the coatings. On these defect areas where steel is directly exposed to the electrolyte solution, calcareous deposits precipitate. The formation of corrosion products on top of the coating and calcareous deposits on the defects provide an additional diffusion barrier for O_2, which results in a lower self-corrosion of TSA coatings. By VAOCP and EIS measurements, the beneficial effect of these deposits to mitigate corrosion was corroborated by revealing a mixed activation-diffusion controlled dissolution mechanism of the TSA coating. In addition, a decrease in the kinetics of the cathodic reaction by increasingly hindered diffusion results in a reduction in TSA corrosion rates. The analysis of EIS data of TSA samples was carried out by fitting the Randles EEC. This leads to the hypothesis that the TSA-steel interface is not taking part in the electrochemical processes, and thus, steel corrosion is completely hindered.

Characterization of corrosion deposits revealed the formation of a corrosion product layer on top of TSA. Cross-sectional analysis of the coatings revealed Al corrosion products filling the pores, although no major corrosion was observed on the TSA-steel interface. In addition, hydrotalcite was identified on top of the coating by Raman and XRD analysis. On top of the defect, the formation of the well-known calcareous deposits made of brucite and aragonite was confirmed.

From the combination of electrochemical data collected through several electrochemical techniques and surface analysis of the samples afterwards, a detailed corrosion mechanism of TSA samples has been shown for fully immersed conditions in marine environments. This can help to optimise the design of offshore structures by improving long-term predictions based on validated data.

Author statement

Rosa Grinon-Echaniz: Conceptualization, Methodology, Investigation, Formal Analysis, Validation, Writing – Original Draft. **Philippe Refait**: Conceptualization, Methodology, Formal Analysis, Validation, Reviewing and Editing. **Marc Jeannin**: Conceptualization, Methodology, Formal Analysis, Validation, Reviewing and Editing. **Rene Sabot**: Conceptualization and methodology. **Shiladitya Paul**: Conceptualization, Supervision, Reviewing and Editing. **Rob Thornton**: Supervision, Reviewing and Editing.

Declaration of Competing Interest

The authors declare that they have no known competing financial interests or personal relationships that could have appeared to influence the work reported in this paper.

Acknowledgements

The authors gratefully acknowledge financial support from the Centre for Doctoral Training in Innovative Metal Processing (IMPaCT) funded by the UK Engineering and Physical Sciences Research Council (EPSRC), grant reference EP/L016206/1.

This publication was made possible by the sponsorship and support of Lloyd's Register Foundation, a charitable foundation helping to protect life and property by supporting engineering-related education, public engagement and the application of research. The work was enabled through, and undertaken at, the National Structural Integrity Research Centre (NSIRC), a postgraduate engineering facility for industry-led research into structural integrity established and managed by TWI through a network of both national and international Universities.

The raw data required to reproduce these findings are available to download from [https://doi.org/10.25392/leicester.data.13953824].

References

[1] W.H. Hartt, 2012 frank newman speller award: Cathodic protection of offshore structures-history and current status, Corrosion. 68 (2012) 1063–1075, https://doi.org/10.5006/0010-9312-68.12.1063.

[2] H.S. Lee, M.A. Ismail, H.B. Choe, Arc thermal metal spray for the protection of steel structures: An overview, Corros. Rev. 33 (2015) 31–61, https://doi.org/10.1515/corrrev-2014-0055.

[3] M.F. Montemor, Functional and smart coatings for corrosion protection: a review of recent advances, Surf. Coatings Technol. 258 (2014) 17–37, https://doi.org/10.1016/j.surfcoat.2014.06.031.

[4] B. Syrek-gerstenkorn, S. Paul, A. Davenport J, Sacrificial thermally sprayed aluminium coatings for marine environments : a review, Coatings 10 (2020) 267.

[5] A. López-Ortega, R. Bayón, J.L. Arana, Evaluation of protective coatings for offshore applications. Corrosion and tribocorrosion behavior in synthetic seawater, Surf. Coatings Technol. 349 (2018) 1083–1097, https://doi.org/10.1016/j.surfcoat.2018.06.089.

[6] V.R.S.S.á Brito, I.N. Bastos, H.R.M. Costa, Corrosion resistance and characterization of metallic coatings deposited by thermal spray on carbon steel, Mater. Des. 41 (2012) 282–288, https://doi.org/10.1016/j.matdes.2012.05.008.

[7] K.P. Fischer, W.H. Thomason, T. Rosbrook, J. Murali, Performance history of thermal-sprayed aluminum coatings in offshore service, Mater. Perform. 34 (1995) 27–35.

[8] W.H. Thomason, Offshore corrosion protection with thermal-sprayed aluminum, in: Proc. Annu. Offshore Technol. Conf., 1985-May, 1985, pp. 125–131, https://doi.org/10.4043/4971-ms.

[9] H.S. Lee, J.K. Singh, M.A. Ismail, C. Bhattacharya, A.H. Seikh, N. Alharthi, R. R. Hussain, Corrosion mechanism and kinetics of Al-Zn coating deposited by arc thermal spraying process in saline solution at prolong exposure periods, Sci. Rep. 9 (2019) 1–17, https://doi.org/10.1038/s41598-019-39943-3.

[10] R.G. Echaniz, S. Paul, R. Thornton, Effect of seawater constituents on the performance of thermal spray aluminum in marine environments, Mater. Corros. (2019) 1–9, https://doi.org/10.1002/maco.201810764.

[11] A. López-Ortega, J.L. Arana, E. Rodríguez, R. Bayón, Corrosion, wear and tribocorrosion performance of a thermally sprayed aluminum coating modified by plasma electrolytic oxidation technique for offshore submerged components protection, Corros. Sci. 143 (2018) 258–280, https://doi.org/10.1016/j.corsci.2018.08.001.

[12] H.S. Lee, J.K. Singh, J.H. Park, Pore blocking characteristics of corrosion products formed on Aluminum coating produced by arc thermal metal spray process in 3.5 wt.% NaCl solution, Constr. Build. Mater. 113 (2016) 905–916, https://doi.org/10.1016/j.conbuildmat.2016.03.135.

[13] W.H. Hartt, C.H. Culberson, S.W. Smith, Calcareous deposits on metal surfaces in seawater - a critical review, Corrosion 40 (1984) 609–618, https://doi.org/10.5006/1.3581927.

[14] Y. Yang, J. Scantlebury, E. Koroleva, A study of calcareous deposits on cathodically protected mild steel in artificial seawater, Metals (Basel). 5 (2015) 439–456, https://doi.org/10.3390/met5010439.

[15] C. Barchiche, C. Deslouis, D. Festy, O. Gil, P. Refait, S. Touzain, B. Tribollet, Characterization of calcareous deposits in artificial seawater by impedance techniques: 3 - Deposit of CaCO3 in the presence of Mg(II), Electrochim. Acta 48 (2003) 1645–1654, https://doi.org/10.1016/S0013-4686(03)00075-6.

[16] C. Deslouis, D. Festy, O. Gil, G. Rius, S. Touzain, B. Tribollet, Characterization of calcareous deposits in arti®cial sea water by impedance techniques - I. Deposit of CaCO 3 without Mg(OH)2, Electrochim. Acta 43 (1998) 1891–1901.

[17] C. Deslouis, D. Festy, O. Gil, V. Maillot, S. Touzain, B. Tribollet, Characterization of calcareous deposits in artificial sea water by impedances techniques: 2-deposit of Mg(OH)2 without CaCO3, Electrochim. Acta 45 (2000) 1837–1845, https://doi.org/10.1016/S0013-4686(99)00403-X.

[18] O.Ø. Knudsen, H. Askestad, R. Aanesen, Repair Coatings for Thermally Sprayed Aluminium, Eurocorr, 2016.

[19] N. Ce, S. Paul, Thermally sprayed aluminum coatings for the protection of subsea risers and pipelines carrying hot fluids, Coatings 6 (2016) 58, https://doi.org/10.3390/coatings6040058.

[20] G. Quale, L. Årtun, M. Iannuzzi, R. Johnsen, Cathodic protection by distributed sacrificial anodes – a new cost- effective solution to prevent corrosion of subsea structures, Corros. NACE 2017 (2017) 1–15.

[21] R. Akkouche, C. Rémazeilles, M. Jeannin, M. Barbalat, R. Sabot, P. Refait, Influence of soil moisture on the corrosion processes of carbon steel in artificial soil: active area and differential aeration cells, Electrochim. Acta 213 (2016) 698–708, https://doi.org/10.1016/j.electacta.2016.07.163.

[22] C. Rahal, M. Masmoudi, R. Abdelhedi, R. Sabot, M. Jeannin, M. Bouaziz, P. Refait, Olive leaf extract as natural corrosion inhibitor for pure copper in 0.5 M NaCl solution: a study by voltammetry around OCP, J. Electroanal. Chem. 769 (2016) 53–61, https://doi.org/10.1016/j.jelechem.2016.03.010.

[23] K. Nişancioğlu, Corrosion and protection of aluminum alloys in seawater. Corros. Behav. Prot. Copp. Alum. Alloy. Seawater, 2007, pp. 145–155, https://doi.org/10.1533/9781845693084.4.145.

[24] H. Ezuber, A. El-Houd, F. El-Shawesh, A study on the corrosion behavior of aluminum alloys in seawater, Mater. Des. 29 (2008) 801–805, https://doi.org/10.1016/j.matdes.2007.01.021.

[25] F.Sd. Silva, J. Bedoya, S. Dosta, N. Cinca, I.G. Cano, J.M. Guilemany, A. V. Benedetti, Corrosion characteristics of cold gas spray coatings of reinforced aluminum deposited onto carbon steel, Corros. Sci. 114 (2017) 57–71, https://doi.org/10.1016/j.corsci.2016.10.019.

[26] G. Kear, B.D. Barker, F.C. Walsh, Electrochemical corrosion of unalloyed copper in chloride media–a critical review, Corros. Sci. 46 (2004) 109–135, https://doi.org/10.1016/S0010-938X(02)00257-3.
[27] E. Abedi Esfahani, H. Salimijazi, M.A. Golozar, J. Mostaghimi, L. Pershin, Study of corrosion behavior of Arc sprayed aluminum coating on mild steel, J. Therm. Spray Technol. 21 (2012) 1195–1202, https://doi.org/10.1007/s11666-012-9810-x.
[28] T.Y. Yung, T.C. Chen, K.C. Tsai, W.F. Lu, J.Y. Huang, T.Y. Liu, Thermal spray coatings of Al, ZnAl and Inconel 625 alloys on SS304L for anti-saline corrosion, Coatings. 9 (2019), https://doi.org/10.3390/coatings9010032.
[29] M.E. Orazem, B. Tribollet, Electrochemical Impedance Spectroscopy, 2008.
[30] C. Deslouis, M.C. Lafont, N. Pebere, D. You, Corrosion inhibition of pure iron in neutral solutions by electrochemical techniques, Corros. Sci. 34 (1993) 1567–1579, https://doi.org/10.1016/0010-938X(93)90032-C.
[31] M. Sancy, Y. Gourbeyre, E.M.M. Sutter, B. Tribollet, Mechanism of corrosion of cast iron covered by aged corrosion products: application of electrochemical impedance spectrometry, Corros. Sci. 52 (2010) 1222–1227, https://doi.org/10.1016/j.corsci.2009.12.026.
[32] N.A. Ce, N.S. Zulkfli, S. Paul, The effect of thermally sprayed aluminum (TSA) coating damage on the mechanism of calcareous deposit formation on steel in boiling seawater, NACE - Int. Corros. Conf. Ser. (2016) 2566–2576.
[33] R.L. Frost, A.W. Musumeci, W.N. Martens, M.O. Adebajo, J. Bouzaid, Raman spectroscopy of hydrotalcites with sulphate, molybdate and chromate in the interlayer, J. Raman Spectrosc. 36 (2005) 925–931, https://doi.org/10.1002/jrs.1385.
[34] S.J. Palmer, R.L. Frost, Characterization of bayer hydrotalcites formed from bauxite refinery residue liquor, Ind. Eng. Chem. Res. 50 (2011) 5346–5351, https://doi.org/10.1021/ie1018194.
[35] K. Ben Mabrouk, T.H. Kauffmann, H. Aroui, M.D. Fontana, Raman study of cation effect on sulfate vibration modes in solid state and in aqueous solutions, J. Raman Spectrosc. 44 (2013) 1603–1608, https://doi.org/10.1002/jrs.4374.